A strategy to improve the structural performance of non-crimp fabric thin-ply laminates

Arteiro, A., Catalanotti, G., Xavier, J., Linde, P., & Camanho, P. P. (2018). A strategy to improve the structural performance of non-crimp fabric thin-ply laminates. *Composite Structures*, *188*, 438-449. https://doi.org/10.1016/j.compstruct.2017.11.072

Published in:
Composite Structures

Document Version:
Peer reviewed version

Queen's University Belfast - Research Portal:
Link to publication record in Queen's University Belfast Research Portal

A strategy to improve the structural performance of non-crimp fabric thin-ply laminates

A. Arteiro, G. Catalanotti, J. Xavier, P. Linde, P.P. Camanho

PII: S0263-8223(17)33909-0
DOI: https://doi.org/10.1016/j.compstruct.2017.11.072
Reference: COST 9138

To appear in: *Composite Structures*

Please cite this article as: Arteiro, A., Catalanotti, G., Xavier, J., Linde, P., Camanho, P.P., A strategy to improve the structural performance of non-crimp fabric thin-ply laminates, *Composite Structures* (2017), doi: https://doi.org/10.1016/j.compstruct.2017.11.072

A strategy to improve the structural performance of non-crimp fabric thin-ply laminates

A. Arteiro[a,*], G. Catalanotti[b], J. Xavier[c,d], P. Linde[e], P.P. Camanho[a,c]

[a] *DEMec, Faculdade de Engenharia, Universidade do Porto, Rua Dr. Roberto Frias, s/n, 4200-465 Porto, Portugal*
[b] *School of Mechanical and Aerospace Engineering, Queen's University Belfast, Belfast, BT9 5AH, UK*
[c] *INEGI, Instituto de Ciência e Inovação em Engenharia Mecânica e Engenharia Industrial, Rua Dr. Roberto Frias, 400, 4200-465 Porto, Portugal*
[d] *CITAB, Universidade de Trás-os-Montes e Alto Douro, Engenharias I, Apartado 1013, 5001-801 Vila Real, Portugal*
[e] *AIRBUS Operations GmbH, Kreetslag 10, 21129 Hamburg, Germany*

Abstract

The enhanced mechanical performance of thin-ply laminates results from their ability to delay the onset of damage typically observed in composite materials. However, in notched structures, subcritical damage growth causes beneficial stress redistributions in the vicinity of the notch, blunting the stress concentration. Precluding these damage mechanisms, as in thin-ply laminates, may potentially lead to inferior notched responses. To obviate this limitation of thin-ply laminates, a strategy based on the combination of standard grade 0° plies and thin transverse and off-axis plies is analysed in this paper. A detailed study of the effect of 0° ply blocking is carried out, with particular emphasis on the blunting mechanisms and notched response. Tests on scaled notched panels loaded in tension, with notch sizes between 6 mm and 30 mm, show that the combination of standard grade 0° ply blocks with thin transverse and off-axis plies promotes localised fibre-matrix splitting, which acts as an important notch blunting mechanism, while preventing matrix cracking and delamination. This results in an improved notched response and superior large damage capability. It is also shown that thicker 0° ply blocks provide higher stability in com-

*Corresponding author. Tel.: +351 220414049.
Email address: aarteiro@fe.up.pt (A. Arteiro)

posite bolted joints, while the thin transverse and off-axis plies contribute for matrix-dominated damage suppression, resulting in an improved bolt-bearing response. The improvements of the large damage capability and bolt-bearing performance are obtained without compromising the superior unnotched tensile and compressive strengths intrinsic to thin-ply laminates.

Keywords: Polymer-matrix composites (PMCs), Thin plies, Mechanical testing, Size effects, Mechanically-fastened joints

1. Introduction

Thin-ply laminates[1] are known for their enhanced mechanical performance, attributed to the ability to delay the onset of the matrix-dominated damage mechanisms typically observed in conventional composite materials. This damage suppression capability results in an enhanced unnotched strength [1–4], improved compressive response [2, 3], and higher fatigue resistance [1, 2, 4, 5]. However, the delay of damage onset may lead to an inferior notched response [4] due to the suppression of the notch blunting mechanisms that cause local stress redistribution and reduce the stress concentration in the vicinity of the notch. Nevertheless, studies focused on minimising, or even eliminating this disadvantage without compromising the enhanced mechanical performance of thin plies are unfortunately scarce.

Recently, Furtado et al. [6] presented an experimental study about the effect of ply-level hybridisation on the tensile unnotched and notched response of composite laminates. They showed that combining thin off-axis and transverse plies with thicker 0° plies results in an enhanced notched behaviour without compromising the unnotched and fatigue responses. The standard grade 0° plies promote localised longitudinal split cracking in the regions of high stress concentration in the vicinity of the notch, resulting in a stress redistribution along

[1] Thin-ply laminates are defined as those composed by plies with thickness lower than 100 μm.

the loading direction that delays unstable fracture of the notched laminates, increasing their notched strength when compared with laminates with thin 0° plies.

Based on these observations, a detailed study of the effect of 0° ply blocking on the blunting mechanisms and notched response of thin-ply laminates is presented. To prevent the occurrence of matrix cracking and delamination, spread-tow thin plies were chosen to design a structural laminate based on a baseline of the aerospace industry. Focus is then placed on the understanding of how 0° ply blocking can be efficiently used to improve the structural integrity of thin-ply laminates without compromising their intrinsically high unnotched strengths. With this objective, a detailed experimental programme is presented. Tests were carried out on two stacking sequences, with dispersed and blocked 0° plies. The unnotched response of both laminates was evaluated in tension and in compression. Then, two important design drivers for aerospace applications — the tensile residual strength (large damage capability) and the bearing strength — are studied in detail to understand the effects of laminate design on the complex behaviour of structural details. Finally, a detailed discussion on the relevant features that govern the structural response of thin-ply laminates and the effect of 0° ply thickness is presented.

2. Material selection and manufacturing

T700GC/M21 C-Ply^{TM} bi-angle non-crimp fabrics (NCFs) from Chomarat, with an areal weight of 75 g/m^2 per layer, were used in the present experimental campaign. Each layer is made of 12k tow-spread T700GC carbon fibres, pre-plied and mechanically sewn with fine stitching yarns. Two configurations were used in the present work, (0/45) and (0/−45) bi-angle layers. Both configurations were pre-impregnated with HexPly® M21 toughened epoxy resin from Hexcel.

A stacking sequence of bi-angle NCFs was defined based on a damage tolerance optimised baseline laminate for aerospace applications, with *dispersed* 0°

plies. An alternative stacking sequence was also defined, but with *blocked* 0° plies. Table 1 shows the stacking sequences definition, where n is the number of repetitions, and the 0° fibre orientation is coincident with the loading direction. Both stacking sequences are oriented, 0°-dominated *hard laminates*, and, following standard design rules, they are both balanced and symmetric. Due to the latter restriction — laminate symmetry — both C-Ply$^{\mathrm{TM}}$ NCF configurations had to be used to reproduce the stacking sequences presented in Table 1. Table 2 shows the C-Ply$^{\mathrm{TM}}$ NCF lay-up sequences.

[Table 1 about here.]

[Table 2 about here.]

In total, four laminates were investigated, with $n = 1$ for the tensile tests and $n = 2$ for the compressive tests. The former had a nominal laminate thickness of 1.8 mm and the latter a nominal laminate thickness of 3.6 mm.

Thanks to the pre-plied off-axis plies, these laminates were manufactured by two-axis hand lay-up (in the 0° and 90° directions), reducing substantially the time spent with the lay-up process. They were then prepared for curing in a vacuum bag and cured in an autoclave. The autoclave cure cycle was defined by setting a heat-up rate of 2°C/min from room temperature to 180°C, holding at 180°C for 120 min and cooling down at a rate of 2°C/min. A gauge autoclave pressure of 4 bar was applied throughout the cure cycle. After curing, each specimen was cut to the nominal dimensions using a diamond-coated disk.

3. Experimental programme

3.1. Unnotched tension and compression tests

To assess the effect of 0° ply blocking on the plain strengths and failure modes of thin-ply laminates loaded in tension and in compression, unnotched specimens were tested to failure. Following the ASTM D3039/D3039M – 14 test standard [7], unnotched specimens with a nominal width (W) of 25 mm and a nominal length (L_{s}) of 300 mm were tested in tension. Hydraulic grips were

used to clamp the specimens to the test frame, and the gauge length (L) set to 150 mm. In selected specimens, 2 mm thick, 75 mm long aluminium tabs were used to assess the effect of clamping on the test results.

In compression, unnotched specimens with $W = 25$ mm and $L_s = L = 305$ mm were tested. A special test rig designed to prevent buckling was used in the compression tests, based on the ASTM D6484/D6484M – 14 test standard [8]. The alignment of the clamping system with the axis of the testing machine was performed using two guiding pins with a diameter of 6 mm close to the ends of the specimens.

3.2. Centre-notched tension tests and notch size effect study

In the design of structural composite parts, the understanding of the mechanical performance and structural integrity of composite materials in the presence of stress concentrations is of great importance. In general, due to a *size effect* on the notched strength, the same laminate can exhibit distinct material behaviours depending on coupon size, from a small-notch, "*strength-dominated*" response, to a large-notch, "*toughness-dominated*" response [9]. Such strength dependence on size must be well understood if strength data from small coupons are intended to be used in the design of large load-bearing structures [10–14]. In the present work, Centre-Notched Tension (CNT) tests were performed on scaled specimens to study the evolution of damage mechanisms in thin-ply laminates with *dispersed* and *blocked* 0° plies. Table 3 shows the CNT size effect test matrix. The width-to-notch length ratio was kept constant and equal to 6 in all specimens.

[Table 3 about here.]

Hydraulic grips were used to hold and apply the tensile load to the test specimens. However, because the 82 mm-wide hydraulic grips were narrower than the largest CNT specimen configurations (see Table 3), aluminium tabs, 2 mm thick and 100 mm long, were used to increase the rigidity of the clamped regions.

3.3. Mechanically fastened joints

The behaviour of composites in bolted joints differs considerably from that of metals. The quasi-brittle nature of composite materials requires more detailed analysis to address the different failure modes occurring in the vicinity of the fasteners. In composites, the stress concentrations dictate the components static strength to a larger extent than in metals due to the absence of yielding, conducting to less efficient joints. In addition, the bearing strength of a composite laminate depends significantly on the lateral support provided in the bearing region. Following the ASTM D5961/D5961M − 13 test standard [15], double-shear bearing tests were performed on the *dispersed* and *blocked* laminates to assess the effect of 0° ply blocking on the structural performance of mechanically fastened joints.

Bolt-bearing and pin-bearing tests [15] were performed using specimens with a nominal hole diameter $d = 6$ mm, end distance-to-hole diameter ratio $e/d = 6$, width-to-hole diameter ratio $W/d = 6$, and nominal length $L_s = 215$ mm. In the bolt-bearing tests, a bolt M6 was used with a washer subjected to a "finger-tight" clamping pressure, corresponding to a fastener torque $T = 2.2$ Nm [15]. In the pin-bearing tests, a 6 mm diameter pin was used to load the bearing hole (no clamping pressure).

Even though bearing failure is, in practice, the most common failure mode in composite mechanically fastened joints, when the hole diameter is large compared with the width of the specimen, or when the bolt spacing in a multi-hole bolted joint is comparatively small, net-tension failure is likely to occur, which can drastically change the strength of the joint [16]. Therefore, net-tension tests were also performed in the present work to study the effect of 0° ply blocking on the net-tension failure mode of composite bolted joints. This is an important structural test, specified by several design guidelines in aeronautics, because, as a geometry-dependent feature often used directly in the analysis methods, it is required in the derivation of in-plane laminate allowables [9]. Specimens with a nominal hole diameter $d = 6$ mm, end distance-to-hole diameter ratio $e/d = 6$, nominal length $L = 215$ mm, and nominal widths (W) of 9 mm and 12 mm were

tested. A bolt M6, subjected to a torque $T = 2.2$ Nm ("finger-tight" clamping pressure [15]), with a washer was used to load the bearing hole.

The end of the specimen far from the bearing hole was fixed using a bolted clamping rig. Grinding paper was inserted between the specimens and the grip to improve the load transfer capability and prevent sliding. The alignment of the longitudinal axis of the gripped specimen with the test direction was performed using a guiding pin with a diameter of 4 mm.

3.4. Specimen preparation and test conditions

The guiding holes in the compression and bearing tests were obtained using a conventional drilling machine. The notches of the CNT tests were milled using a 1 mm drill bit, ensuring a distance of 1 mm between the notch faces. In all cases, carbon-epoxy sacrificial plates were used at the top and bottom faces of the specimens to avoid damage during the machining process.

The unnotched and notched tension tests were performed in an Instron 4208 electro-mechanical universal testing machine with a load capacity of 300 kN equipped with a 300 kN load cell, and the unnotched compression tests in a servo-hydraulic MTS 810 testing machine with a load capacity of 250 kN using a 250 kN load cell. The bearing and net-tension tests were performed in a servo-hydraulic MTS 810 testing machine with a load capacity of 100 kN and a 100 kN load cell. All tests were performed under displacement control, at a controlled speed of 1.0 mm/min.

3.5. Instrumentation

The use of full-field optical techniques to monitor damage and fracture phenomena can be extremely useful in identifying and understanding the complex failure behaviour of composite materials [3, 17–20]. The digital image correlation (DIC) technique was used in this experimental programme to measure the in-plane displacement and strain fields. These data can then be used to identify strain/stress concentrations, transverse cracking onset and propagation in the

surface plies, and to observe the differences in damage formation and propagation in the numerous coupon configurations studied in the present work. All measurements were performed by means of a single camera, using the ARAMIS DIC-2D v6.0.2 system developed by GOM [21]. The adopted configuration is summarised in Table 4.

[Table 4 about here.]

4. Experimental results

4.1. Tensile and compressive plain strengths

When subjected to tensile loads, both laminates exhibited a linear response up to ultimate failure. Monitoring the data from DIC, it was observed that, prior to ultimate failure, transverse matrix cracking had not extended across the width of the specimens, remaining confined to the free edges (Fig. 1). When compared with conventional laminates with the same epoxy resin [18], transverse cracking was strongly delayed in this case, attributed to an *in situ* effect [22]. This clearly shows the potential of thin transverse plies to suppress subcritical failure mechanisms.

[Figure 1 about here.]

All tensile specimens exhibited a fibre-dominated pull-out failure mode, with the failure section perpendicular to the loading direction (Fig. 2). However, the extent of delamination and pulled-out fibre bundles was slightly higher in the *blocked* laminate, suggesting a higher susceptibility to grow subcritical damage mechanisms. In fact, 0° ply blocking originates higher interlaminar stresses at the adjacent interfaces, which become more susceptible to delamination and split cracking. Also, in the *blocked* laminate, some of the adjacent NCF bi-angle layers were stacked with relative ply orientations of 90° (Table 1), conducting to higher interlaminar stresses between these plies, which contributed for the onset of delamination at these interfaces.

[Figure 2 about here.]

Table 5 shows the average results for the tensile unnotched strengths, X_T^L, of the *dispersed* and *blocked* laminates calculated dividing the peak loads measured by the load cell, by the cross-section area of the specimens. Table 5 also shows the coefficients of variation of the unnotched tests. As can be observed, the tensile strengths of the tested laminates differ by just 2.3%, a difference within the variation of the tests. It can be concluded, therefore, that the tensile strength of both laminates is virtually the same.

[Table 5 about here.]

In compression, both laminates exhibited a nonlinear behaviour (Fig. 3). This suggests that permanent damage or generalised plastic deformation developed before ultimate failure (see also Ref. [3]).

[Figure 3 about here.]

Interestingly, Fig. 3 shows that damage onset occurred earlier in the *dispersed* laminate. However, after damage initiation, the *dispersed* laminate exhibited a progressive failure response. A series of load drops, which increased as the specimen approached ultimate failure, can be observed. It is also noted that these load drops occurred at an approximately constant peak remote stress, suggesting that a gradual propagation of the compressive failure mechanisms occurred in this laminate.

The *blocked* laminate, on the other hand, was characterised by fast damage propagation. Soon after damage initiation, all specimens exhibited a catastrophic failure response (Fig. 3), indicating that the compressive failure mechanisms that led to ultimate failure of the *blocked* laminate are characterised by unstable propagation.

All compression specimens exhibited a net-section failure mode. Failure of both laminates was characterised by a complex combination of damage mechanisms, including fibre kinking, brittle shear-driven fibre fracture, wedge transverse matrix cracking, crushing and delamination (Fig. 4), whose sequence was

not easy to identify. In some specimens, multiple fracture planes, inclined with respect to the laminate mid-plane, were observed, revealing the catastrophic type of failure of this test configuration.

[Figure 4 about here.]

The *dispersed* laminate had apparently a brittler failure mode (Fig. 4a), as the occurrence of fibre kinking was reduced, and a high degree of abrasion of the inclined crack surfaces, typical of shear-driven brittle compressive failure [23], was observed. Nevertheless, despite its brittler nature, damage initiated earlier and propagated progressively (see Fig. 3). This can be attributed to gradual matrix-dominated crushing, and to through-thickness confinement of shear-driven fibre fracture of the thin 0° plies promoted locally by the surrounding transverse and off-axis plies and globally by the ASTM test rig used.

The *blocked* laminate exhibited a more irregular failure surface (Fig. 4b), dominated by fibre kinking. This indicates that thicker 0° plies have higher susceptibility to grow kink bands before ultimate compressive failure. After formation, the kink bands propagated quickly through the thickness, resulting in the unstable response shown in Fig. 3.

Nonetheless, it is interesting to note that, despite the different failure morphologies of the *dispersed* and *blocked* laminates, the compressive unnotched strengths, X_C^L, are remarkably similar (see Table 5). This suggests that final longitudinal compressive failure was not governed by the sequence of damage mechanisms that led to failure of the 0° plies.

4.2. Notch size effects and large damage capability

Small load drops were observed in all CNT tests, becoming more important as the size of the specimens increased. These load drops were caused by the development of a fracture process zone ahead of the notch tips, including fibre breakage. Both laminates exhibited a fibre-dominated pull-out failure mode (Fig. 5). Surface split cracking of the ±45° plies, severe internal split cracking of the 0° plies, fibre pull-out, and localised delaminations were observed at the

vicinity of the notch tips. As the size of the specimens increased, the damage process zone ahead of the notch tips became larger and more diffuse. Longitudinal split cracks propagated quickly after slow damage growth from the notch tips along the off-axis directions. After extensive diffuse damage propagation, catastrophic intralaminar fracture occurred either perpendicular to or at an angle of $-45°$ with the loading direction, conducting to final failure. This type of diffuse damage growth before brittle, unstable propagation of an intralaminar crack was substantially different from the brittle failure modes observed on quasi-isotropic specimens with similar geometries and similar size range [3, 20, 24].

[Figure 5 about here.]

The surface strain fields obtained with DIC showed that, in general, the onset of intralaminar damage growth from the notch tips started earlier in the *dispersed* laminate (Figs. 6–9). Surface damage restraining in the *blocked* laminate can be attributed to stress relaxation caused by internal damage growth, which delayed the onset of through-thickness intralaminar damage.

[Figure 6 about here.]

[Figure 7 about here.]

[Figure 8 about here.]

[Figure 9 about here.]

X-ray radiographs from selected tests interrupted at approximately 95% of the peak load (Figs. 10 and 11) show that split cracking started in the off-axis and $0°$ plies where the fibre direction is tangent to the semi-circular boundary of the notch tips, as reported for open-hole specimens loaded in tension [25, 26]. Delaminations with a triangular shape connecting the off-axis split cracks can also be identified. On the other hand, transverse matrix cracking in the $90°$ plies is precluded in both laminates, which can be attributed to an *in situ* effect in the transverse tensile strength [22].

[Figure 10 about here.]

[Figure 11 about here.]

A detailed analysis of the radiographs taken from the different scaled geometries showed that the off-axis and 0° split cracks tended to grow at a similar pace in the *blocked* laminate (Fig. 11). However, in the *dispersed* laminate (Fig. 10), the off-axis splits generally started earlier and propagated slightly faster than the 0° splits.

Table 6 shows the mean ultimate remote stresses of the CNT tests and corresponding coefficients of variation. These results are summarised in Fig. 12. As expected, in general, as the size of the specimens increases, the tensile notched strength decreases. It is also observed that the tensile notched strengths of the *blocked* laminate are higher than the notched strengths of the *dispersed* laminate.

[Table 6 about here.]

[Figure 12 about here.]

4.3. Performance of mechanically fastened joints

The bolt-bearing tests exhibited a linear response up to approximately 50% of the maximum bearing stress, followed by a small kink before becoming nonlinear (Fig. 13). A similar response was already reported in Ref. [3].

[Figure 13 about here.]

All bolt-bearing specimens exhibited a bearing failure mode, resulting from local compressive damage in the bearing hole region. Besides local compressive failure and crushing of the load-bearing surface, which are the typical damage mechanisms [3, 27], transverse and split cracking of the outer 90° plies was also observed after permanent deformation of the hole. No relevant difference was observed between the specimens of the *dispersed* and *blocked* laminates after testing.

Table 7 shows the average test results and respective coefficients of variation for the bearing strengths of the *dispersed* and *blocked* laminates according to the most common definitions used in the literature: average bearing stress at the onset of nonlinearity, average bearing stress for an offset bearing strain of 2%, average bearing stress at the first load drop, and average maximum bearing stress. The bearing stress (σ^{br}) and the offset bearing strain ($\varepsilon^{br}_{\text{offset}}$) were determined following the ASTM D5961/D5961M – 13 test standard [15].

[Table 7 about here.]

Interestingly, the *blocked* laminate exhibits higher bearing strengths than the *dispersed* laminate, independently of the bearing strength definition employed (see also Fig. 13). The average bearing stress of the *blocked* laminate at the onset of nonlinearity ($\sigma^{br}_{\text{nonlin}}$) and at the first load drop ($\sigma^{br}_{\text{drop}}$) are respectively 13.5% and 7.1% higher than in the *dispersed* laminate. Adopting a hard laminate configuration with blocked 0° plies resulted, therefore, in an improved bearing response with respect to the onset and propagation of local compressive damage.

Optical through-thickness micrographs of the bearing planes of interrupted bolt-bearing tests (Figs. 14a and 15a) showed that the onset of nonlinearity is associated with the initiation of wedge matrix cracking (*dispersed* and *blocked* laminates) and fibre kinking (*blocked* laminate). The *dispersed* laminate (Fig. 14a) had apparently the ability to delay the initiation of fibre kinking, as the first nonlinearity was mostly due to matrix cracking in the transverse and off-axis plies. This suggests that thinner 0° plies have the ability to delay the onset of compressive longitudinal fracture.

[Figure 14 about here.]

[Figure 15 about here.]

At the first load drop (Figs. 14b and 15b), wedge matrix cracking and fibre kinking had already propagated considerably in both laminates. The interaction of these damage mechanisms led to the formation of through-thickness

shear cracks, whose propagation conducted to further load drops and permanent hole deformation. However, in the *dispersed* laminate, the propagation of severe damage apparently occurred earlier than in the *blocked* laminate. A possible explanation for the delay of through-thickness damage propagation in the *blocked* laminate is the additional stability imposed by the thicker 0° plies in the region confined by the lateral support provided by the bolt/washer assembly, which increases locally the laminate compressive strength.

To assess the effect of the confining pressure, pin-bearing tests were also performed. As expected, all specimens exhibited a bearing failure mode. Transverse and split cracking in the outer 90° plies was also observed. Both laminates exhibited a linear response up to approximately 97% of the maximum bearing stress (Fig. 16). At failure, a large load drop occurred, reducing the applied bearing stress to approximately 50% of its maximum value. In the absence of the confining pressure, once microscopic damage mechanisms, such as matrix cracking and fibre kinking, start to form, they quickly propagate into macrocracks and crushing due to the lack of lateral support, reducing considerably the joint load-carrying capacity.

[Figure 16 about here.]

Table 7 shows the average test results and respective coefficients of variation for the pin-bearing tests. Unlike the results for the bolted joints, there is virtually no difference between the results of the *dispersed* and *blocked* laminates when subjected to pin-bearing loads.

Figure 16 and Table 7 also show that the lateral support provided by the bolt/washer assembly in the bolted joints effectively delays the onset of nonlinearity to values above the maximum bearing stress observed in the tests with pinned joints. In addition, it is clear that the delay in damage initiation provided by the bolt/washer assembly is more effective in the *blocked* laminate, confirming the observation that the additional stability of the thicker 0° plies in the region subjected to the through-thickness confining pressure can delay the onset and propagation of severe through-thickness damage.

To study the effect of joint geometry, net-tension tests were also performed. All net-tension specimens exhibited a fibre-dominated pull-out net-tension failure mode (Fig. 17). Delaminations with a triangular shape extended from the hole edge across the ligament section, connected to matrix cracks in the 45° plies starting where the fibre direction is tangent to the hole free edge. Whereas the 9 mm wide specimens of both laminates exhibited a linear response up to the maximum bearing stress (Fig. 18a), followed by catastrophic net-tension failure, the 12 mm wide specimens exhibited a small nonlinearity close to the maximum bearing stress, in some cases including small load drops (Fig. 18b). This nonlinear response was caused by the onset of bearing damage at the hole boundary tangent to the bearing plane. As can be observed in Table 8, the maximum bearing stresses of the 12 mm wide specimens of both laminates are slightly higher than the corresponding bearing stresses at the onset of nonlinearity determined in the bolt-bearing tests (Table 7). Nevertheless, it can be assumed that the low extent of local compressive damage in the hole boundary did not affect the final net-tension strength of the tested specimens.

[Figure 17 about here.]

[Figure 18 about here.]

[Table 8 about here.]

Table 8 also shows that the maximum bearing stresses of the 9 mm wide *dispersed* and *blocked* laminates do not differ substantially. The maximum bearing stress of the larger 12 mm wide *blocked* laminate is 4.3% higher than the maximum bearing stress of the *dispersed* laminate. Due to the small ligament width of the 9 mm wide specimens, propagation of damage mechanisms such as matrix cracking in the off-axis plies and delamination along the short ligament section occurred rapidly in both laminates, making any differences in the blunting effects unnoticeable. A larger ligament width, as in the 12 mm wide specimens, resulted in a superior blunting effect in the *blocked* laminate due to the clustered 0° plies, delaying unstable net-section failure and conducting to a slightly higher

net-tension bearing strength, in line with the results obtained with open-hole tension [6] and centre-notched tension (Sect. 4.2).

5. Observations and discussion

Laminates with thicker plies, or ply blocking, have been associated with low plain strengths [1, 4, 18, 28–31], mostly attributed to the development of matrix cracking in the transverse and off-axis plies, and to extensive delamination growth before failure of the 0° plies. These damage mechanisms are a consequence of lower *in situ* strengths of the thick transverse and off-axis plies and higher interlaminar stresses between adjacent plies. The matrix cracks and delamination fronts act as stress concentration points on the load carrying 0° plies, leading to early laminate failure.

The present work shows that restricting ply blocking to the 0° plies has a negligible effect on the ultimate unnotched strengths of the laminates. In tension, transverse cracking and delamination are effectively delayed, potentiating the load carrying capacity of the 0° plies, independently of their thickness and position in the laminate. In compression, despite the different failure morphology and extent of damage in the 0° plies, the absence of matrix-dominated damage mechanisms, especially delamination, led to similar compressive unnotched strengths in the *dispersed* and *blocked* laminates.

But the same damage mechanisms that contribute for early laminate failure in smooth coupons, act as notch blunting mechanisms in notched structures, in particular when loaded in tension [3, 6, 18, 25, 26, 32]. Because these damage mechanisms are precluded in laminates with thin plies, these laminates usually show higher notch sensitivity than conventional laminates. On the other hand, in laminates with sufficiently thick plies, delamination becomes the predominant failure mechanism [25, 26]. Delaminations start from the matrix cracks in the transverse and off-axis plies tangent to the notch boundary, due to the low *in situ* strengths, and from the free edges, caused by the high interlaminar stresses. They initially propagate along the interfaces between the transverse and off-axis

plies, and then step through the adjacent interfaces via the transverse and off-axis matrix cracks, reaching the interface with the 0° plies [25, 26]. Delamination then propagates extensively, leading to the loss of structural integrity before failure of the remaining 0° ligaments. Despite an apparent notch insensitivity, the failure morphology and the low unnotched strengths make such laminates unsuitable for structural design.

Furtado et al. [6] showed that, by combining thin transverse and off-axis plies with thick 0° plies, the development of the more detrimental transverse matrix cracks and delaminations could be precluded, while longitudinal fibre-matrix splitting would still be induced in the thick 0° plies at the vicinity of the open hole [14, 28, 33, 34], which act as an important notch blunting mechanism [18, 35]. As a consequence of the induced split cracks, the local stress field changes due to stress relaxation in the vicinity of the notch, reducing the local stress concentration, and delaying unstable intralaminar fracture. This leads to the higher ultimate tensile notched strengths observed.

In the present work, it is shown that the introduction of thick 0° plies in a structural thin-ply laminate can also enhance the tensile notched response of the laminate in the presence of sharp through-thickness cracks. Moreover, such enhanced notched response is valid for a wide range of coupon geometries, from small-notch specimens to large damage capability test panels. With this strategy, the residual strength in the event of service through-penetration damage can be improved over conventional solutions, without compromising the intrinsically high tensile unnotched strength of thin-ply laminates.

In addition to the residual strength of notched laminates, another relevant design driver in many industries, particularly in aerospace, is the resistance to localised damage in overloaded mechanically fastened joints. Thin-ply laminates are reportedly characterised by an outstanding bearing performance when compared with standard-ply laminates [3, 4]. This is mostly attributed to the suppression of subcritical damage in the vicinity of the loaded area promoted by more effective ply constraining, higher *in situ* strengths, and lower interlaminar stresses.

The present work shows that combining thick 0° plies with thin transverse and off-axis plies leads to an over-enhancement of the bearing performance of bolted joints. The thicker 0° plies improve the stability of the laminate in the region confined by the lateral support provided by the bolt/washer assembly, while the thin transverse and off-axis plies delay the onset and propagation of matrix-dominated damage mechanisms. This results in a local increase of the laminate compressive strength.

In the case of pinned joints, without mechanical confinement in the load bearing region, the introduction of the thick 0° plies has a negligible effect on the bearing response of the thin-ply laminate. This shows that the added stability provided by the thick 0° plies in bolted joints is a direct effect of the lateral support provided by the bolt/washer assembly. When the laminate failure mode changes from bearing failure to net-tension failure across the hole section, the same trends observed in open-hole tension are obtained [6]: the thicker 0° plies lead to a superior blunting effect in the hole vicinity, delaying unstable net-section failure, resulting in a slightly higher net-tension bearing strength. These results are particularly important in understanding how the lateral support and joint geometry affect the bearing performance of structural laminates, and how laminates can be designed for improved joint efficiency with thin plies and selective ply-level hybridisation.

It is finally noted that in the presence of high stress gradients, either from remotely loaded laminate panels with through-thickness notches or from locally loaded structural details as in mechanically fastened joints, the use of thin plies along the transverse and off-axis orientations ensures that matrix cracking and delamination preceding ultimate failure can be effectively delayed or even suppressed, contributing for improved unnotched, compressive and fatigue behaviours [1–5]. Combining them with thicker 0° plies to promote notch blunting in tension through fibre-matrix splitting, and to promote longitudinal stability in compression provides a laminate design approach for improved structural response, with great potential to increase the design allowables for many structural applications, in particular in the aerospace industry.

6. Conclusions

With the aim to improve the structural response of composite laminates, spread-tow thin-ply NCFs were chosen to design a structural laminate based on a baseline of the aerospace industry. To improve local blunting near geometrical stress concentrations, a detailed study of the effect of 0° ply blocking on the structural behaviour of an aerospace-grade thin-ply laminate was carried out in the present work.

In spite of small differences in the damage mechanisms that preceded ultimate failure, the tensile and the compressive unnotched strengths of thin-ply laminates with *dispersed* and *blocked* 0° plies were virtually insensitive to the 0° ply thickness. However, enhanced centre-notched strengths over a wide range of coupon sizes were observed in the laminate with *blocked* 0° plies. In this laminate, the onset of intralaminar damage growth and ultimate failure were delayed due to higher stress relaxation in the vicinity of the notch tips caused by larger longitudinal split cracks in the 0° plies, blunting the notch and reducing the local stress concentration, in agreement with previous observations in the literature [14]. Finally, an improved overall bearing performance was observed in the laminate with *blocked* 0° plies in bolted joints, attributed to the additional stability of the thicker 0° plies in the region confined by the lateral support provided by the bolt/washer assembly, which effectively delayed the onset and propagation of localised compressive damage. However, in the case of pinned joints (no bolt fastened), no relevant difference was observed between the laminates with *dispersed* and *blocked* 0° plies, confirming the effect of the clamping pressure on the additional stability of the thicker 0° plies. When subjected to a net-tension failure mode, a superior blunting effect was observed in sufficiently wide specimens of the laminate with *blocked* 0° plies, which delayed unstable net-section failure, leading to a slightly higher net-tension strength, in line with the results obtained for open-hole tension in Ref. [6] and centre-notched tension in the present work.

These results show that a wise combination of thin transverse and off-axis

plies with thicker 0° plies leads to improvements of the structural response of composite laminates, without affecting the in-plane elastic response or the laminate plain strengths, in agreement with the conclusions from Ref. [6]. In addition, the use of thin plies ensures that matrix cracking and delamination preceding ultimate failure can be effectively delayed or even suppressed, which is known to have a positive effect on the unnotched, compressive and fatigue response of composite laminates [1–5].

Acknowledgements

This work was funded by AIRBUS under project 2genComp — second generation Composites. The authors gratefully acknowledge the support provided by AIRBUS.

The authors are also grateful to Chomarat (Le Cheylard, France) for providing the non-crimp fabrics used in the experimental test campaign reported in this paper, and to Prof. Josep Costa and his team at the University of Girona for performing the X-ray radiographs.

The first author would like to thank the financial support provided by FCT – Fundação para a Ciência e a Tecnologia through National Funds in the scope of project MITP-TB/PFM/0005/2013.

The last author gratefully acknowledges the funding of Project NORTE-01-0145-FEDER-000022 – SciTech – Science and Technology for Competitive and Sustainable Industries, co-financed by Programa Operacional Regional do Norte (NORTE2020), Fundo Europeu de Desenvolvimento Regional (FEDER).

References

[1] Sihn S, Kim RY, Kawabe K, Tsai SW. Experimental studies of thin-ply laminated composites. Compos Sci Technol 2007;67:996–1008.

[2] Yokozeki T, Aoki Y, Ogasawara T. Experimental characterization of strength and damage resistance properties of thin-ply carbon fiber/toughened epoxy laminates. Compos Struct 2008;82:382–9.

[3] Arteiro A, Catalanotti G, Xavier J, Camanho PP. Notched response of non-crimp fabric thin-ply laminates. Compos Sci Technol 2013;79:97–114.

[4] Amacher R, Cugnoni J, Botsis J, Sorensen L, Smith W, Dransfeld C. Thin ply composites: Experimental characterization and modeling of size-effects. Compos Sci Technol 2014;101:121–32.

[5] Nishikawa Y, Okubo K, Fujii T, Kawabe K. Fatigue crack constraint in plain-woven CFRP using newly-developed spread tows. Int J Fatigue 2006;28:1248–53.

[6] Furtado C, Arteiro A, Catalanotti G, Xavier J, Camanho PP. Selective ply-level hybridisation for improved notched response of composite laminates. Compos Struct 2016;145:1–14.

[7] Standard test method for tensile properties of polymer matrix composite materials, ASTM D3039/D3039M – 14. ASTM International; West Conshohocken, PA, USA; 2014.

[8] Standard test method for open-hole compressive strength of polymer matrix composite laminates, ASTM D6484/D6484M – 14. ASTM International; West Conshohocken, PA, USA; 2014.

[9] CMH-17-3G . Composite Materials Handbook; vol. 3 of 6: Polymer Matrix Composites Materials Usage, Design and Analysis. SAE International; 2012.

[10] Wisnom MR. Size effects in the testing of fibre-composite materials. Compos Sci Technol 1999;59:1937–57.

[11] Bažant ZP. Size effect on structural strength: a review. Arch Appl Mech 1999;69:703–25.

[12] Bažant ZP. Size effect. Int J Solids Struct 2000;37:69–80.

[13] Bažant ZP, Yavari A. Is the cause of size effect on structural strength fractal or energetic-statistical? Engng Fract Mech 2005;72:1–31.

[14] Xu X, Wisnom MR, Mahadik Y, Hallett SR. An experimental investigation into size effects in quasi-isotropic carbon/epoxy laminates with sharp and blunt notches. Compos Sci Technol 2014;100:220–7.

[15] Standard test method for bearing response of polymer matrix composite laminates, ASTM D5961/D5961M – 13. ASTM International; West Conshohocken, PA, USA; 2013.

[16] Catalanotti G, Camanho PP. A semi-analytical method to predict net-tension failure of mechanically fastened joints in composite laminates. Compos Sci Technol 2013;76:69–76.

[17] Laurin F, Charrier JS, Lévêque D, Maire JF, Mavel A, Nuñez P. Determination of the properties of composite materials thanks to digital image correlation measurements. Procedia IUTAM 2012;4:106–15.

[18] Erçin GH, Camanho PP, Xavier J, Catalanotti G, Mahdi S, Linde P. Size effects on the tensile and compressive failure of notched composite laminates. Compos Struct 2013;96:736–44.

[19] Caminero MA, Lopez-Pedrosa M, Pinna C, Soutis C. Damage monitoring and analysis of composite laminates with an open hole and adhesively bonded repairs using digital image correlation. Compos Part B-Eng 2013;53:76–91.

[20] Arteiro A, Catalanotti G, Xavier J, Camanho PP. Large damage capability of non-crimp fabric thin-ply laminates. Compos Part A-Appl S 2014;63:110–22.

[21] GOM International AG. Bremgarterstrasse 89B, CH-8967 Widen, Switzerland; 2000.

[22] Camanho PP, Dávila CG, Pinho ST, Iannucci L, Robinson P. Prediction of in situ strengths and matrix cracking in composites under transverse tension and in-plane shear. Compos Part A-Appl S 2006;37:165–76.

[23] Gutkin R, Pinho ST, Robinson P, Curtis PT. On the transition from shear-driven fibre compressive failure to fibre kinking in notched CFRP laminates under longitudinal compression. Compos Sci Technol 2010;70:1223–31.

[24] Camanho PP, Catalanotti G. On the relation between the mode I fracture toughness of a composite laminate and that of a 0° ply: Analytical model and experimental validation. Engng Fract Mech 2011;78:2535–46.

[25] Green BG, Wisnom MR, Hallett SR. An experimental investigation into the tensile strength scaling of notched composites. Compos Part A-Appl S 2007;38:867–78.

[26] Hallett SR, Green BG, Jiang WG, Wisnom MR. An experimental and numerical investigation into the damage mechanisms in notched composites. Compos Part A-Appl S 2009;40:613–24.

[27] Camanho PP, Lambert M. A design methodology for mechanically fastened joints in laminated composite materials. Compos Sci Technol 2006;66:3004–20.

[28] Lavoie JA, Soutis C, Morton J. Apparent strength scaling in continuous ber composite laminates. Compos Sci Technol 2000;60:283–99.

[29] Wisnom MR, Khan B, Hallett SR. Size effects in unnotched tensile strength of unidirectional and quasi-isotropic carbon/epoxy composites. Compos Struct 2008;84:21–8.

[30] Lee J, Soutis C. Measuring the notched compressive strength of composite laminates: Specimen size effects. Compos Sci Technol 2008;68:2359–66.

[31] Soutis C, Lee J. Scaling effects in notched carbon fibre/epoxy composites loaded in compression. J Mater Sci 2008;43:6593–8.

[32] Wisnom MR, Hallett SR. The role of delamination in strength, failure mechanisms and hole size effect in open hole tensile tests on quasi-isotropic laminates. Compos Part A-Appl S 2009;40:335–42.

[33] O'Higgins RM, McCarthy MA, McCarthy CT. Comparison of open hole tension characteristics of high strength glass and carbon fibre-reinforced composite materials. Compos Sci Technol 2008;68:2770–8.

[34] Xu X, Wisnom MR, Mahadik Y, Hallett SR. Scaling of fracture response in Over-height Compact Tension tests. Compos Part A-Appl S 2015;69:40–8.

[35] Iarve EV, Mollenhauer D, Kim R. Theoretical and experimental investigation of stress redistribution in open hole composite laminates due to damage accumulation. Compos Part A-Appl S 2005;36:163–71.

[36] Xavier J, de Jesus AMP, Morais JJL, Pinto JMT. Stereovision measurements on evaluating the modulus of elasticity of wood by compression tests parallel to the grain. Constr Build Mater 2012;26(1):207–15.

[37] Catalanotti G, Xavier J, Camanho PP. Measurement of the compressive crack resistance curve of composites using the size effect law. Compos Part A-Appl S 2014;56:300–7.

List of Figures

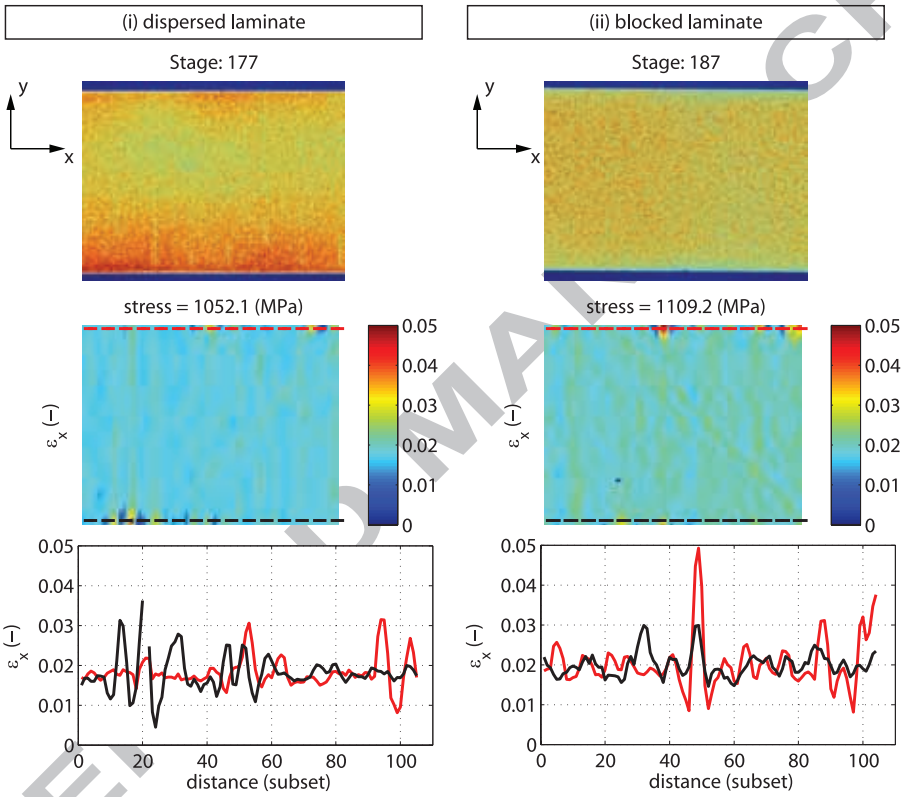

Figure 1: Coloured distributions of grey levels (0–255), longitudinal strain fields, ε_x, and local longitudinal strain measured along the edges of the outer 90° ply of representative unnotched tension test specimens of the (i) *dispersed* and (ii) *blocked* laminates obtained with the DIC technique at the stage prior to ultimate failure. The reference DIC coordinate system is depicted in the figures, where the x-axis is aligned with the loading direction.

(a) *Dispersed* laminate.

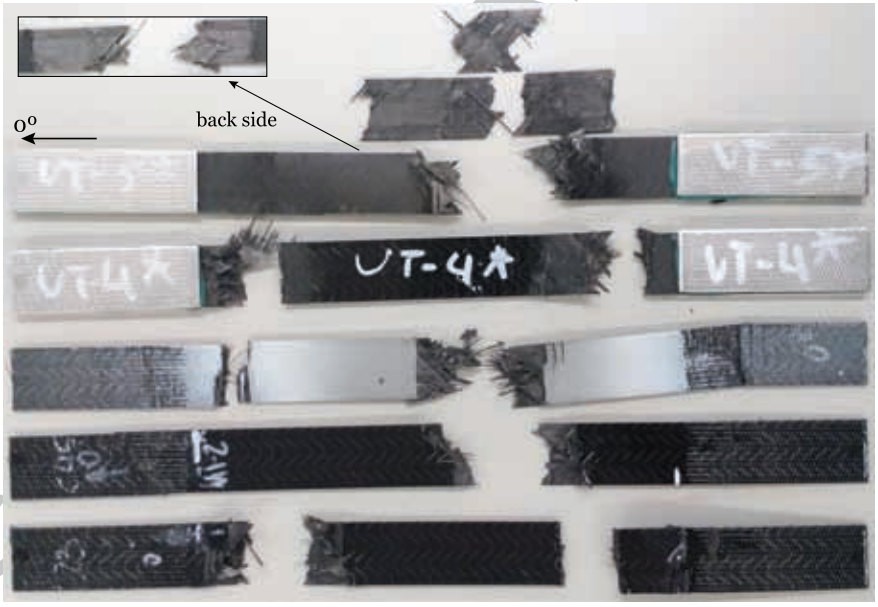

(b) *Blocked* laminate.

Figure 2: Representative unnotched tension test specimens after testing.

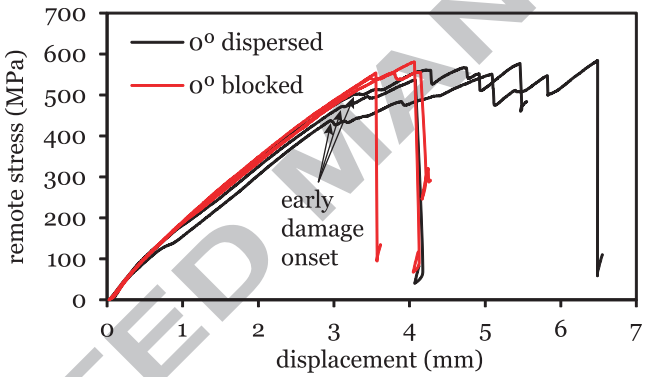

Figure 3: Unnotched compression test results.

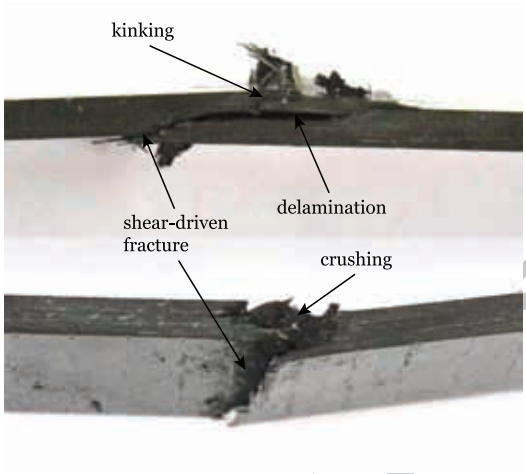

(a) *Dispersed* laminate.

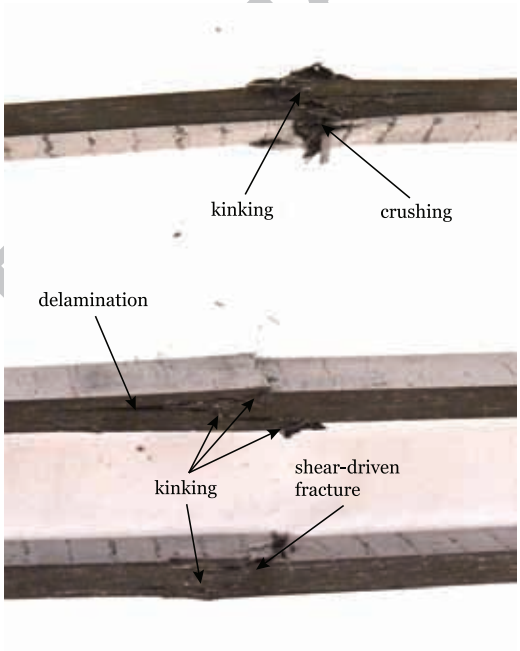

(b) *Blocked* laminate.

Figure 4: Details of the unnotched compression test specimens after testing.

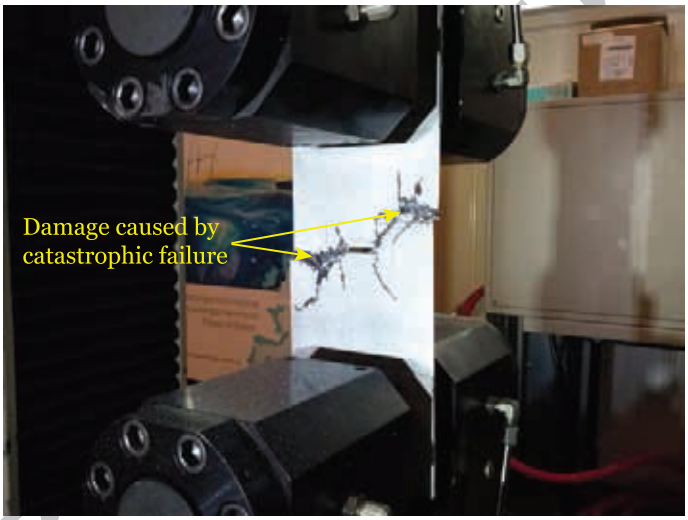

Figure 5: Representative 144 mm wide specimen after testing.

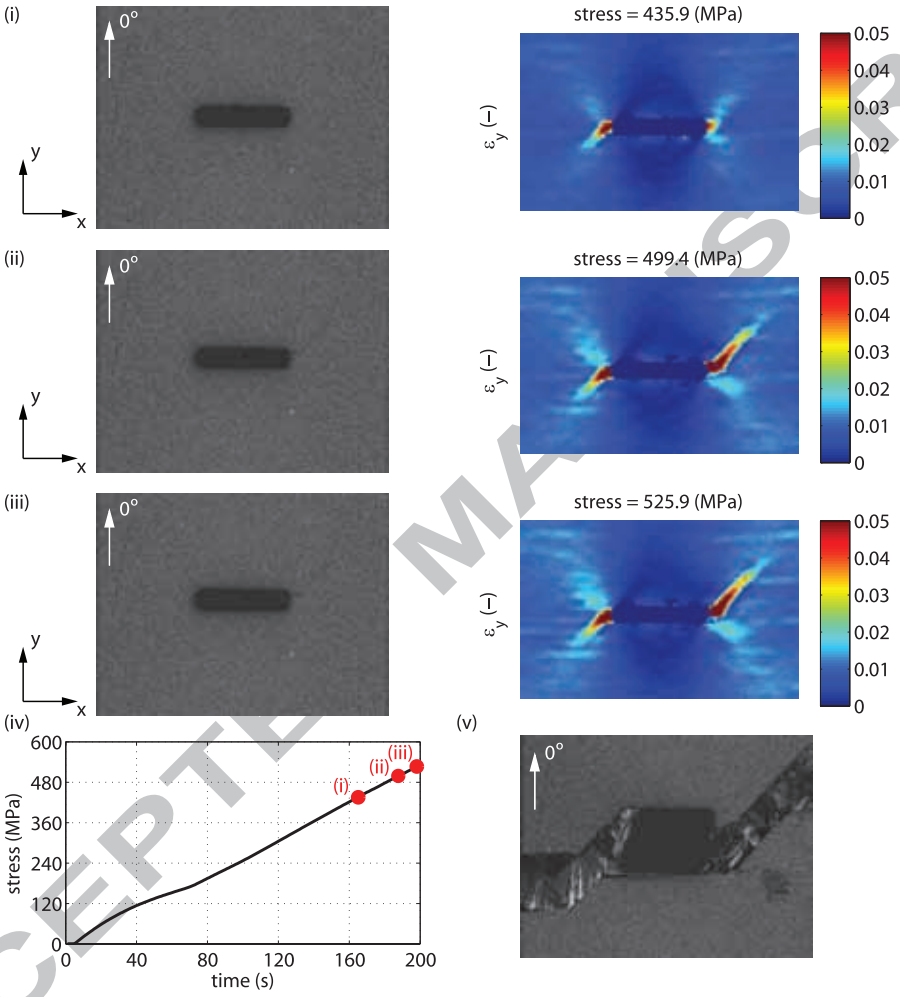

Figure 6: Surface and longitudinal strain field, ε_y, of the outer 90° ply of a representative 36 mm wide *dispersed* CNT test specimen obtained with the DIC system at the stages of (i) onset of transverse cracking, (ii) at 95% of the ultimate remote stress, and (iii) at the ultimate remote stress. (iv) Remote stress-time relation. (v) Surface of the specimen after failure obtained with the DIC image grabbing setup. The reference DIC coordinate system is depicted in the figures, where the y-axis is aligned with the loading direction.

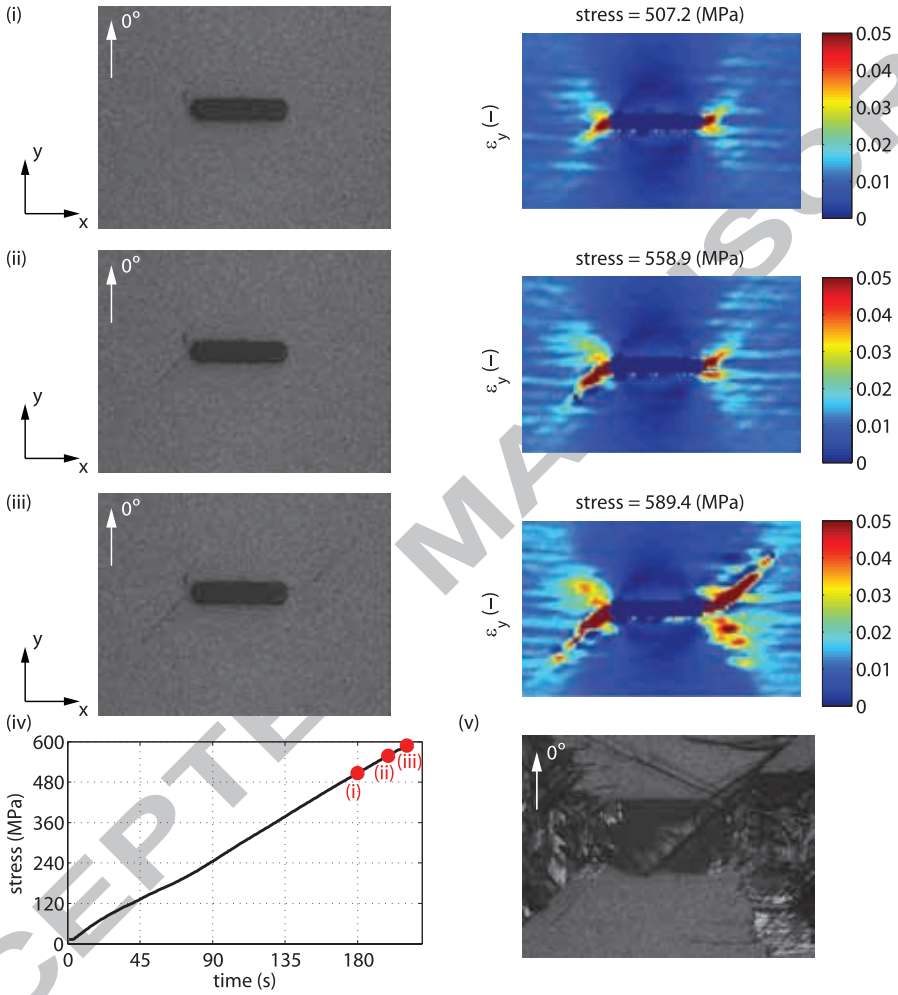

Figure 7: Surface and longitudinal strain field, ε_y, of the outer 90° ply of a representative 36 mm wide *blocked* CNT test specimen obtained with the DIC system at the stages of (i) onset of transverse cracking, (ii) at 95% of the ultimate remote stress, and (iii) at the ultimate remote stress. (iv) Remote stress-time relation. (v) Surface of the specimen after failure obtained with the DIC image grabbing setup. The reference DIC coordinate system is depicted in the figures, where the y-axis is aligned with the loading direction.

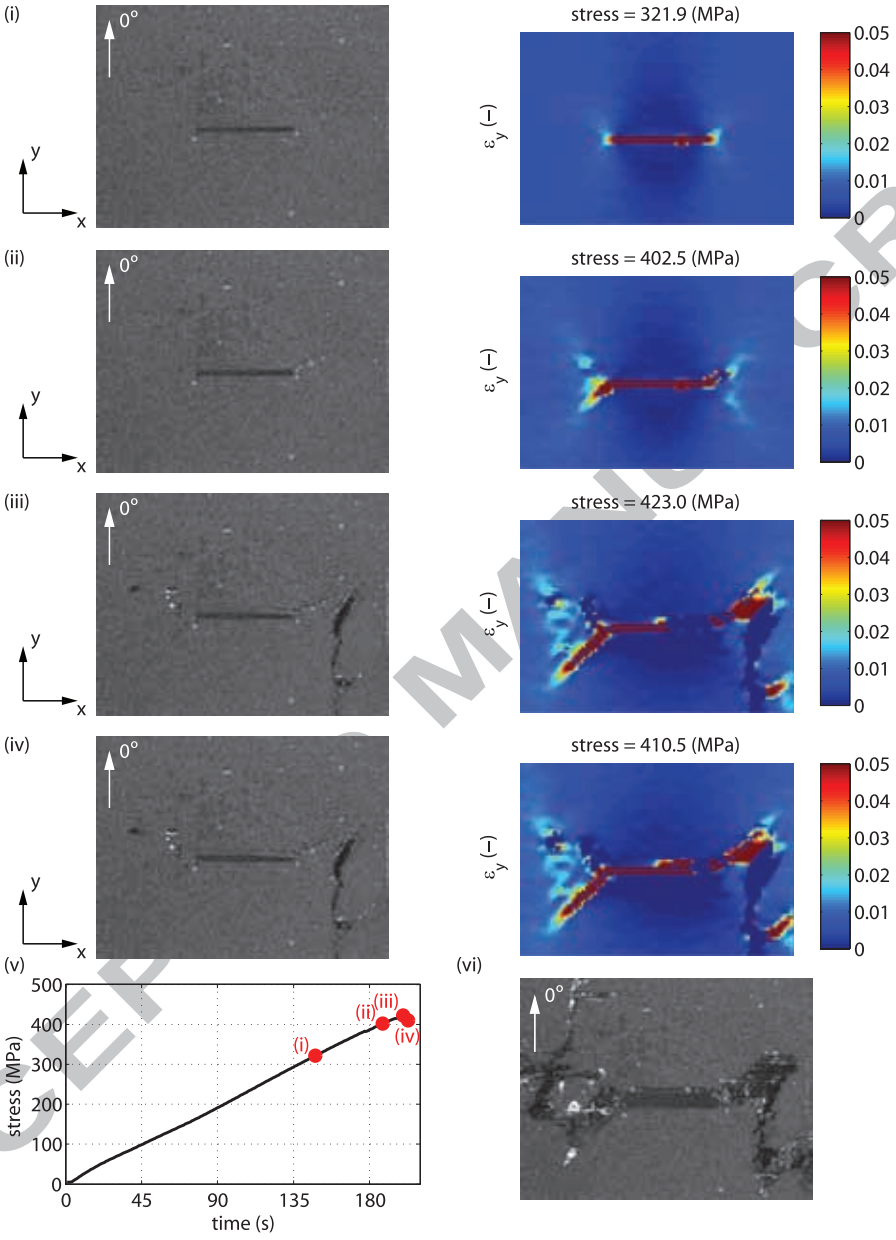

Figure 8: Surface and longitudinal strain field, ε_y, of the outer 90° ply of a representative 144 mm wide *dispersed* CNT test specimen obtained with the DIC system at the stages of (i) onset of transverse cracking, (ii) at 95% of the ultimate remote stress, (iii) at the maximum remote stress, and (iv) just before ultimate failure. (v) Remote stress-time relation. (vi) Surface of the specimen after failure obtained with the DIC image grabbing setup. The reference DIC coordinate system is depicted in the figures, where the y-axis is aligned with the loading direction.

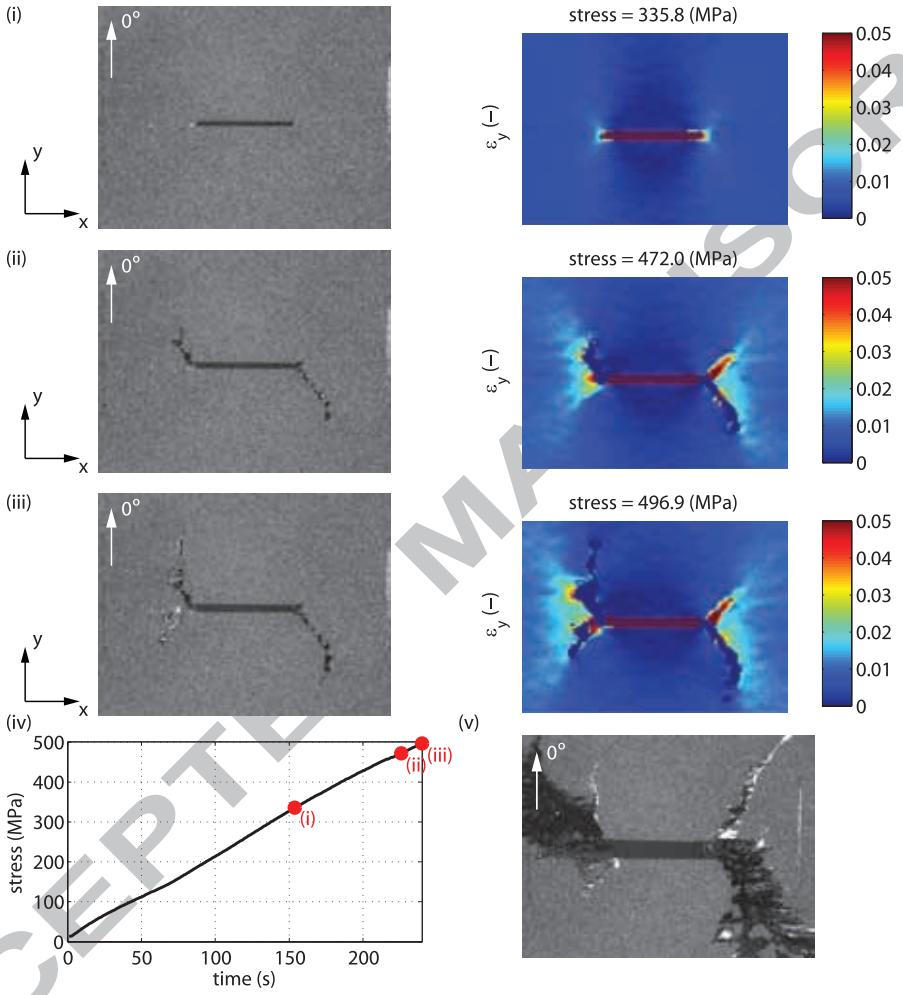

Figure 9: Surface and longitudinal strain field, ε_y, of the outer 90° ply of a representative 144 mm wide *blocked* CNT test specimen obtained with the DIC system at the stages of (i) onset of transverse cracking, (ii) at 95% of the ultimate remote stress, and (iii) at the ultimate remote stress. (iv) Remote stress-time relation. (v) Surface of the specimen after failure obtained with the DIC image grabbing setup. The reference DIC coordinate system is depicted in the figures, where the y-axis is aligned with the loading direction.

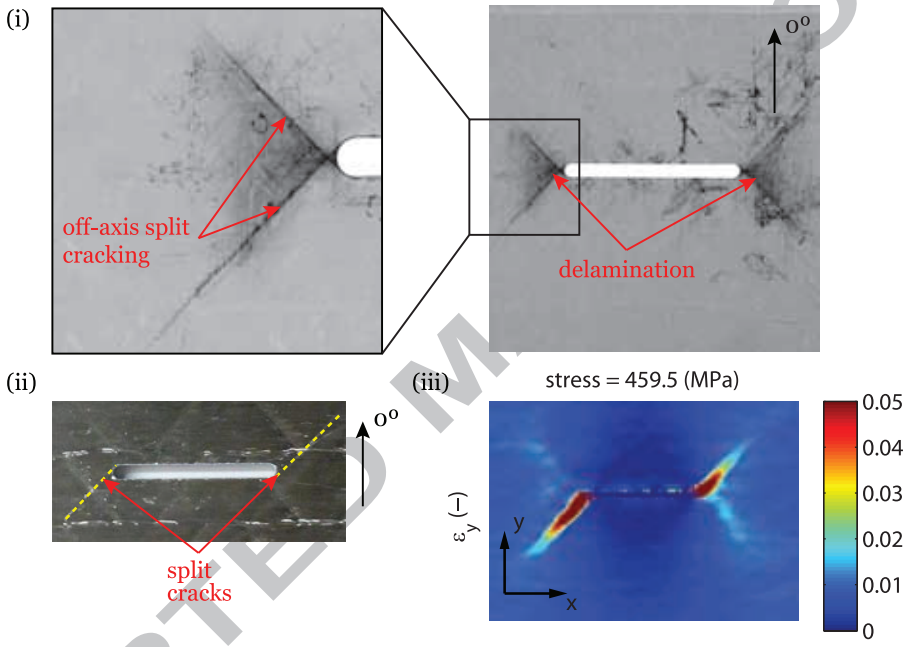

Figure 10: Damage on the 72 mm wide CNT specimen of the *dispersed* laminate after interrupted testing at 95% of the mean ultimate remote stress. (i) X-ray radiographs of the notch and of a detail of the left notch tip (scanning voltage of 45 kV (140 μA) and exposure time of 2 s). (ii) Schematic of the damage identified by external visual inspection. (iii) Longitudinal strain field, ε_y, in the outer 90° ply obtained with the DIC technique (the reference DIC coordinate system is depicted in the figure, where the y-axis is aligned with the loading direction).

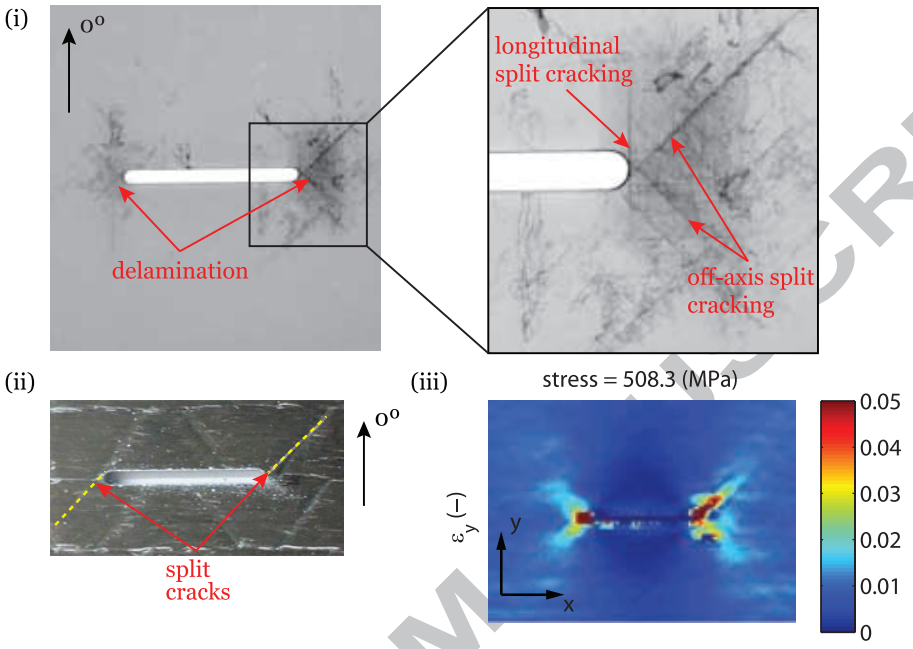

Figure 11: Damage on the 72 mm wide CNT specimen of the *blocked* laminate after interrupted testing at 95% of the mean ultimate remote stress. (i) X-ray radiographs of the notch and of a detail of the right notch tip (scanning voltage of 45 kV (140 μA) and exposure time of 2 s). (ii) Schematic of the damage identified by external visual inspection. (iii) Longitudinal strain field, ε_y, in the outer 90° ply obtained with the DIC technique (the reference DIC coordinate system is depicted in the figure, where the y-axis is aligned with the loading direction).

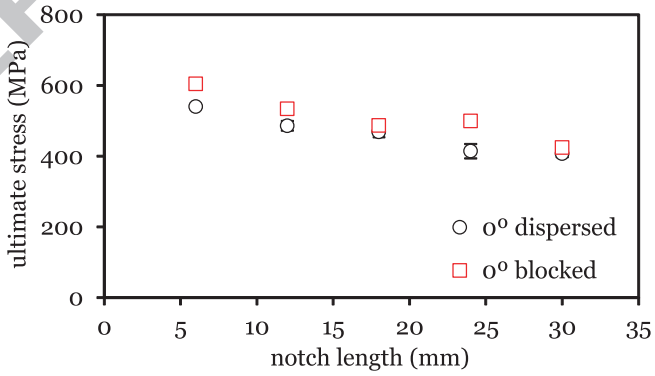

Figure 12: Tensile notched strengths.

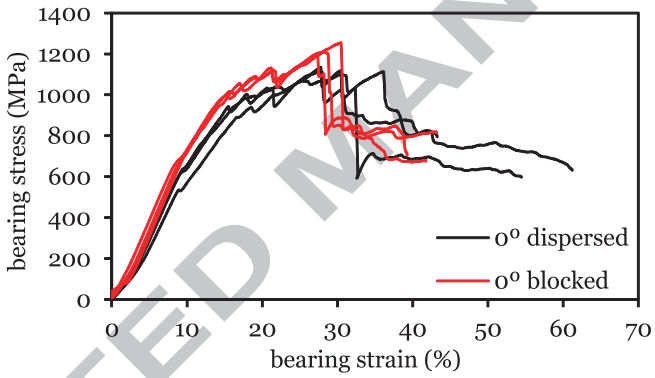

Figure 13: Bearing stress-bearing strain relations for the bolt-bearing tests.

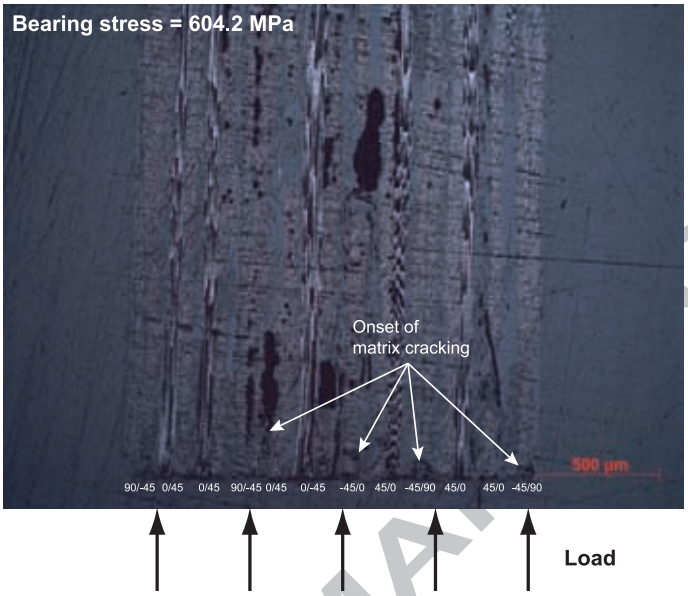

(a) Onset of nonlinearity.

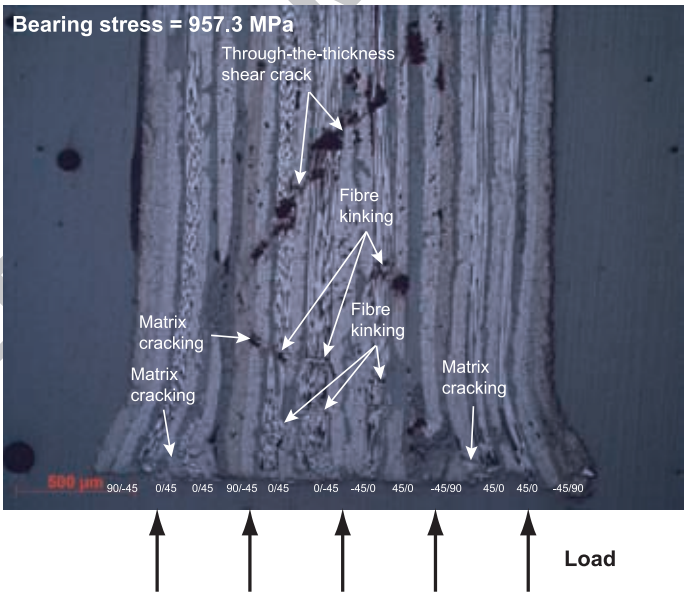

(b) First load drop.

Figure 14: Bearing plane of representative bolt-bearing specimens of the *dispersed* laminate (magnification factor of 5×).

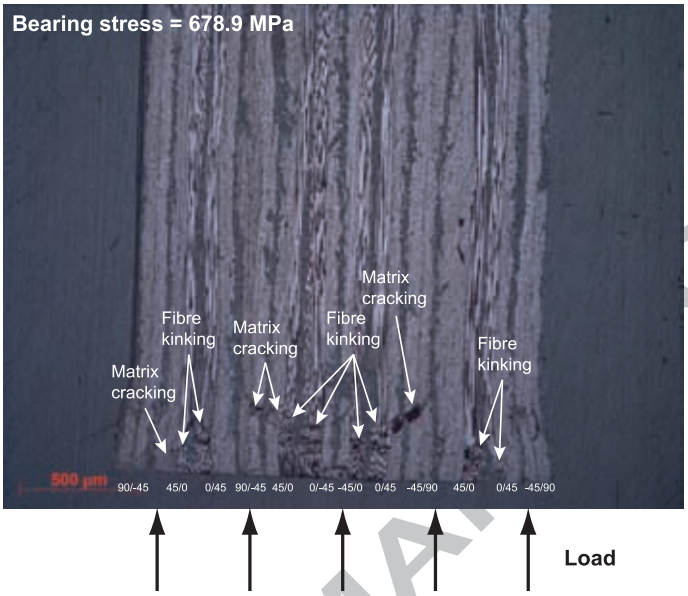

(a) Onset of nonlinearity.

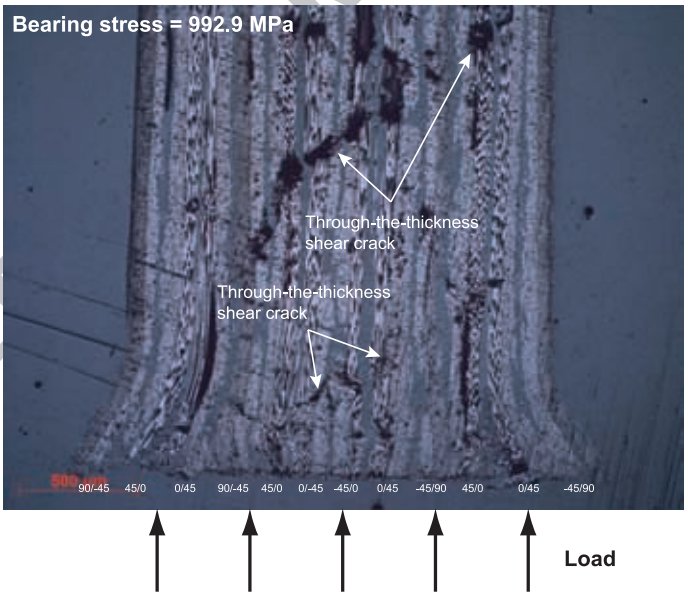

(b) First load drop.

Figure 15: Bearing plane of representative bolt-bearing specimens of the *blocked* laminate (magnification factor of 5×).

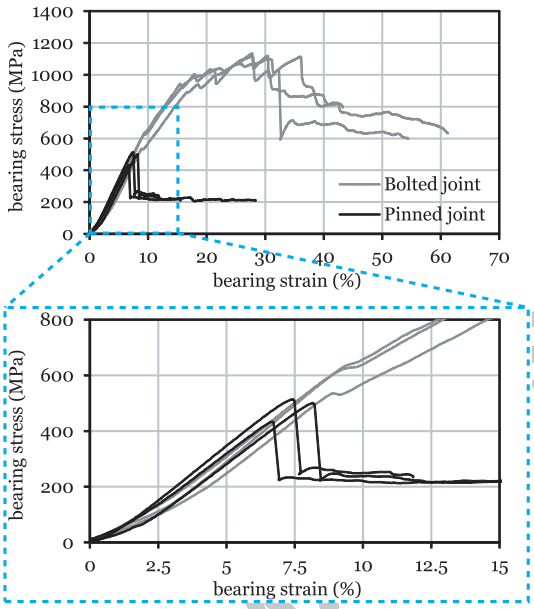

(a) *Dispersed* laminate.

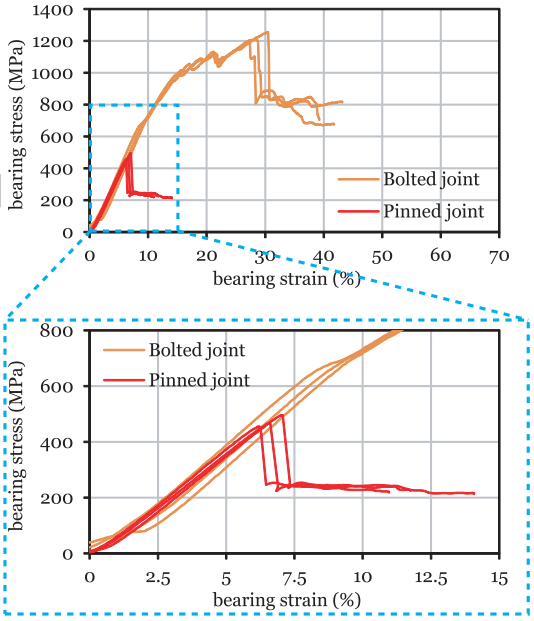

(b) *Blocked* laminate.

Figure 16: Comparison between the bearing stress-bearing strain curves for bolted and pinned joints.

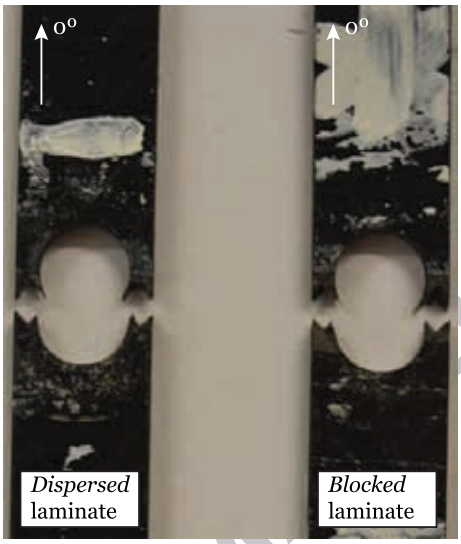

(a) Specimen width: 9 mm (small).

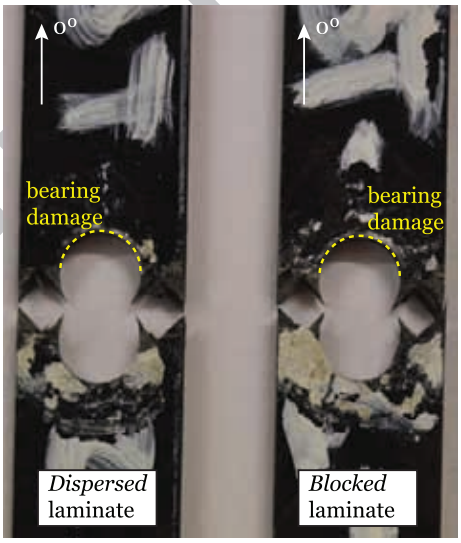

(b) Specimen width: 12 mm (large).

Figure 17: Bearing hole region of representative net-tension specimens after testing.

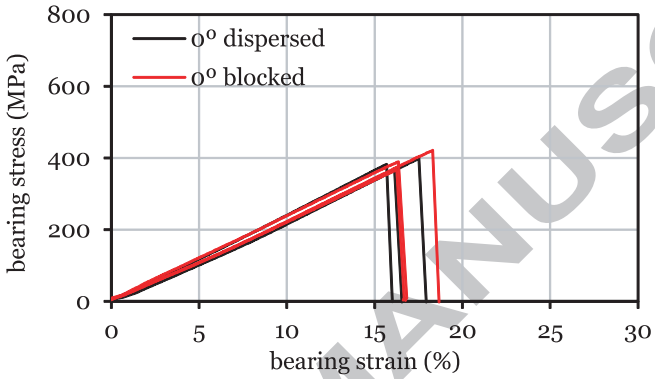

(a) Specimen width: 9 mm (small).

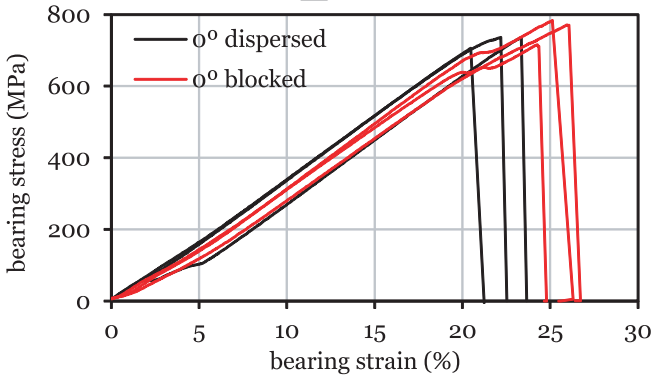

(b) Specimen width: 12 mm (large).

Figure 18: Bearing stress-bearing strain relations for the net-tension tests.

List of Tables

Table 1: Stacking sequence definitions.

Laminate ID	Stacking sequence
dispersed	$[(90/-45)/(\mathbf{0}/45)/(\mathbf{0}/45)/(90/-45)/(\mathbf{0}/45)/(\mathbf{0}/-45)]_{n\mathrm{S}}$
blocked	$[(90/-45)/(45/\mathbf{0})/(\mathbf{0}/45)/(90/-45)/(45/\mathbf{0})/(\mathbf{0}/-45)]_{n\mathrm{S}}$

Table 2: C-Ply$^{\mathrm{TM}}$ NCF lay-up sequences.

Laminate ID	NCF lay-up sequence[†‡]
dispersed	$(\mathrm{A}(90)/\mathbf{A}/\mathrm{A}/\mathrm{A}(90)/\mathbf{A}/\mathrm{B})_n//(\text{-A}/\mathbf{\text{-B}}/\text{-B}(90)/\text{-B}/\mathbf{\text{-B}}/\text{-B}(90))_n$
blocked	$(\mathrm{A}(90)/\mathbf{\text{-B}}/\mathrm{A}/\mathrm{A}(90)/\mathbf{\text{-B}}/\mathrm{B})_n//(\text{-A}/\mathbf{A}/\text{-B}(90)/\text{-B}/\mathbf{A}/\text{-B}(90))_n$

[†] A: (0/45) NCF
[†] A(90): (0/45) NCF rotated 90°: (90/−45)
[†] -A: inverted (0/45) NCF: (−45/0)
[†] -A(90): inverted (0/45) NCF rotated 90°: (45/90)
[‡] B: (0/−45) NCF
[‡] B(90): (0/−45) NCF rotated 90°: (90/45)
[‡] -B: inverted (0/−45) NCF: (45/0)
[‡] -B(90): inverted (0/−45) NCF rotated 90°: (−45/90)

Table 3: CNT size effect test matrix.

Notch length ($2a$)	Width (W)	Specimen length (L_s)	Gauge length (L)
6 mm	36 mm	300 mm	150 mm
12 mm	72 mm	300 mm	150 mm
18 mm	108 mm	400 mm	200 mm
24 mm	144 mm	400 mm	200 mm
30 mm	180 mm	400 mm	200 mm

Table 4: Configuration of the DIC system.

Camera-lens optical system	
CCD camera	Baumer 138 Optronic FWX20
	8-bit
	Resolution: 1624×1236 pixels^2
	Sensor format: 1/1.8”
Lens	Nikon AF Micro-Nikkor 200 mm f/4D IF-ED
	Lens aperture: f/11
DIC measuring parameters	
Subset size	15×15 pixels^2
Subset step	13×13 pixels^2
Strain base length	5×5 subsets^2
Strain validity code	55.0%
Strain computation method	Total
DIC resolution	
Spatial resolution	2×10^{-2} pixels [36, 37]
Strain resolution	0.01-0.04% [36, 37]

Table 5: Laminate unnotched strengths (X_T^L and X_C^L) and coefficients of variation (C.V.).

Results	*Dispersed* laminate	*Blocked* laminate
Tension		
No. specimens	3	5
X_T^L (MPa)	1064	1088
C.V. (%)	1.8	2.2
Compression		
No. specimens	3	3
X_C^L (MPa)	569	566
C.V. (%)	3.7	2.2

Table 6: Tensile notched strengths ($\bar{\sigma}^{\infty}$) and coefficients of variation (C.V.).

Results	Notch length (mm)				
	6	12	18	24	30
***Dispersed* laminate**					
No. specimens	3	3	2	3	3
$\bar{\sigma}^{\infty}$ (MPa)	540	486	469	414	407
C.V. (%)	0.6	2.3	2.3	4.0	1.9
***Blocked* laminate**					
No. specimens	3	3	3	3	3
$\bar{\sigma}^{\infty}$ (MPa)	605	534	487	500	425
C.V. (%)	0.9	1.5	1.7	2.5	3.5

Table 7: Average bolt- and pin-bearing test results and coefficients of variation (C.V.).

Results	*Dispersed* laminate	*Blocked* laminate
No. specimens	3	3
Average bolt-bearing stress at the onset of nonlinearity		
$\sigma^{br}_{\text{nonlin}}$ (MPa)	601	682
C.V. (%)	7.8	2.5
Average bolt-bearing stress for an offset bearing strain of 2%		
$\sigma^{br}_{2\%\text{offset}}$ (MPa)	812	938
C.V. (%)	4.9	1.5
Average bolt-bearing stress at the first load drop		
$\sigma^{br}_{\text{drop}}$ (MPa)	956	1024
C.V. (%)	2.1	2.3
Average maximum bolt-bearing stress		
σ^{br}_{max} (MPa)	1121	1223
C.V. (%)	0.9	1.9
No. specimens	3	3
Average pin-bearing stress at the onset of nonlinearity		
$\sigma^{br}_{\text{nonlin}}$ (MPa)	468	462
C.V. (%)	7.0	3.8
Average maximum pin-bearing stress		
σ^{br}_{max} (MPa)	483	473
C.V. (%)	7.3	3.6

Table 8: Average maximum net-tension bearing stresses ($\bar{\sigma}^{br}$) and coefficients of variation (C.V.).

Results	*Dispersed* laminate	*Blocked* laminate
Specimen width: 9 mm		
No. specimens	3	3
$\bar{\sigma}^{br}$ (MPa)	382	392
C.V. (%)	3.5	5.7
Specimen width: 12 mm		
No. specimens	3	3
$\bar{\sigma}^{br}$ (MPa)	726	757
C.V. (%)	2.0	3.9